DYNAMIC CRACK TIP STRESS FIELDS IN FRACTURE TEST SPECIMENS

A. Shukla* and R. Chona**

**Department of Mechanical Engineering and Applied Mechanics, University of Rhode Island, Kingston, RI 02881, USA*

***Department of Mechanical Engineering, University of Maryland, College Park, MD 20742, USA*

ABSTRACT

Dynamic stress field equations are developed in series form and combined with the multiple-point least-squares method to obtain the relevant stress field parameters from crack tip isochromatic fringe patterns. These parameters are shown to behave in a systematic manner as the crack propagates across different fracture specimens such as the SEN, MCT, and Ring. Particular emphasis is placed on K and σ_{ox} as these parameters are believed to have the most influence on the fracture behavior.

INTRODUCTION

It has been demonstrated [1,2,3] that stress field representations incorporating terms additional to the singularity are frequently necessary if the stress state surrounding the tip of a running crack in a finite plate specimen is to be modeled adequately. A failure to include these terms in the analysis model can seriously affect the ability to obtain accurate and reliable values of the stress intensity factor from experimental data taken in the form of isochromatics, isopachics, caustics, or moire fringes.

The effect of higher-order (or non-singular) terms on K-determination was first studied by Etheridge and Dally [4]. A more detailed study of two and three parameter, static and dynamic stress fields is due to Rossmanith and Irwin [5], in which the authors demonstrated the frequent need for a three-parameter stress field model but did not provide any technique for reliable evaluation of these parameters from experimental data. More recently Chona, Irwin and Shukla [6] presented a method for evaluating the first three parameters of interest from photoelastic data using data points from selected regions of an isochromatic fringe pattern. Several other methods based upon single points or selected data regions have been reviewed in Reference [7].

Sanford and Dally [8] recognized that the use of the full-field information available from photoelastic fracture patterns could be usefully combined with a non-linear, multiple-point, over-deterministic least-squares method to provide a generalized parameter determination procedure. This approach has been combined with generalized series representations for static crack-tip stress fields and applied to isochromatic, isopachic, caustic, and moire fringe data [2,9].

This paper presents the development of generalized stress field equations for plane elastodynamic crack problems and demonstrates how the least-squares methodology can be applied to the evaluation of dynamic fracture parameters. Data is analyzed from dynamic photoelastic experiments performed using three different fracture specimen geometries, namely the Single-Edge-Notched (SEN), Modified-Compact-Tension (MCT) and Ring or C-shaped specimens. The model material in all cases was a brittle, birefringent polyester, Homalite 100, which has been used extensively for dynamic studies of brittle fracture [10,11]. Results are presented for the variation with crack length of the leading terms in a series stress field representation and particular emphasis is placed on the behavior of the stress intensity factor, K, and the uniform stress parallel to the crack line, σ_{ox}, which are believed to have the greatest influence on the fracture process.

DYNAMIC STRESS FIELD REPRESENTATION

Irwin [12] has shown, that for a crack tip stress pattern translating in the positive x-direction at a fixed speed, the dilatation, Δ, and rotation, ω, can be expressed as

$$\Delta = \frac{\partial u}{\partial x} + \frac{\partial v}{\partial y} = A\,(1 - \lambda_1^2)\ \mathrm{Re}\ \Gamma_1(z_1)$$
$$\omega = \frac{\partial v}{\partial x} - \frac{\partial u}{\partial y} = B\,(1 - \lambda_2^2)\ \mathrm{Im}\ \Gamma_2(z_2) \qquad (1)$$

where λ_1, λ_2, z_1, z_2 are defined in Figure 1. Using Hooke's Law

$$\sigma_{xx} = \mu\ [\ A\,(1 + 2\lambda_1^2 - \lambda_2^2)\ \mathrm{Re}\Gamma_1 - 2B\,\lambda_2\ \mathrm{Re}\Gamma_2\ ]$$
$$\sigma_{yy} = \mu\ [-A\,(1 + \lambda_2^2)\ \mathrm{Re}\Gamma_1 + 2B\,\lambda_2\ \mathrm{Re}\Gamma_2\ ] \qquad (2)$$
$$\text{and } \tau_{xy} = \mu\ [-2A\,\lambda_1\ \mathrm{Im}\Gamma_1 + B\,(1 + \lambda_2^2)\ \mathrm{Im}\Gamma_2\ ]$$

where the constants A and B have to be evaluated, after selecting general stress functions, Γ_1 and Γ_2, so as to satisfy the boundary conditions for the crack problem of interest. For the opening mode case, one logical choice is

$$\Gamma_1 = \sum_{j=o}^{j=J} C_j\, z_1^{\,j-1/2} \quad \text{with} \quad \Gamma_2 = \sum_{j=o}^{j=J} C_j\, z_2^{\,j-1/2} \qquad (3)$$

The leading coefficient, C_o, is related to the stress intensity factor, $K = C_o\sqrt{2\pi}$, and the leading term is the familiar inverse-square-root stress singularity. The symmetry condition requires that $B = 2\lambda_1 A/(1+\lambda_2^2)$.

An alternative choice is

$$\Gamma_1 = \sum_{m=o}^{m=M} D_m\, z_1^{\,m} \quad \text{with} \quad \Gamma_2 = \sum_{m=o}^{m=M} D_m\, z_2^{\,m} \qquad (4)$$

which is required to completely describe the stress field in specimens with finite boundaries in a manner analogous to that demonstrated to be the case in the static problem [1,2]. The boundary conditions on the crack faces require that $B = A(1+\lambda_2^2)/2\lambda_2$. The leading term, D_o, gives rise to a superposed constant stress in the direction of crack propagation which is similar to the σ_{ox}-term in Irwin's static near-field equations [13]. This term can also be regarded as the far-field biaxiality correction factor studied extensively by Liebowitz and his co-workers [14] for the static case.

PARAMETER DETERMINATION USING THE LEAST-SQUARES METHOD

Equations (2)-(4), when combined with the stress-optic law, can be used to relate the fringe order, N, at any point in an isochromatic field with the unknown real coefficients, C_j and D_m, through:

$$(Nf_\sigma/2t)^2 = \tau_{max}^2 = 1/4(\sigma_{yy} - \sigma_{xx})^2 + \tau_{xy}^2 \qquad (5)$$

where f_σ is the fringe sensitivity of the model material and t is the model thickness. The first step in the analysis of an isochromatic fringe pattern is to take a region around the crack tip from the experimental pattern being analyzed, extract a large number of individual data points and determine the coordinates and fringe order at each point. These data points are then used as inputs to an over-determined system of non-linear equations of the form of equation (5) and solved in a least-squares sense for the unknown coefficients. As a final check, the best-fit set of coefficients is used to reconstruct the fringe pattern over the region of data acquisition, to ensure that the computed solution set does, in fact, predict the same stress distribution as that observed experimentally.

When analyzing dynamic stress patterns, the data acquisition region is usually restricted to that portion of the stress pattern that can be seen to translate with moderate changes in order to approximate the constant crack-speed assumption. In cases where the crack tip is approaching a specimen boundary, the data region should be restricted to no more than 1/4 to 1/3 the distance to the boundary. The number of coefficients necessary for an adequate representation of the stress field over the data acquisition region can be estimated by examining, as a function of the number of parameters, the average fringe order error, the values of the leading coefficients, and the reconstructed (computer-generated) fringe pattern corresponding to a given set of coefficients. Stability of the error term and leading coefficients, as well as a good visual match between experimental and reconstructed patterns indicates convergence to a satisfactory solution.

A typical example consisting of an experimental fringe pattern and the reconstructed pattern is shown in Figure 2. A total of 60 data points have been taken over a region of radius 0.15W, centered at the crack tip, which is located at an a/W of 0.52 in a Ring specimen. The reconstructed pattern is based upon a six-parameter stress field representation (C_o,D_o,C_1,D_1,C_2,D_2), and can be seen to match the salient features of the experimental pattern over the sampled region around the crack tip. Figure 3 shows the decrease in error and increased stability of C_o, D_o and C_1 that occurs with an increasing order model for the example shown in Figure 2.

The accuracy of parameter determination that is made possible by this technique allows the extension of photoelastic methods to problems such as fracture specimen characterization [15,16], permits the calculation of quantities such as the singularity-dominated zone size in different specimen geometries [16,17] and is essential if photoelastically obtained results are to be used for a better understanding of complicated phenomena such as crack branching and crack curving [18,19].

CRACK PROPAGATION STUDIES IN SEN, MCT, AND RING SPECIMENS

The geometries and relative sizes of the specimens used in this study are shown in Figure 4. These geometries were selected because they collectively characterize all phases of crack propagation. The SEN specimen, when tested with center-pin-loading, has an increasing K-field and can be used to study accelerating and high velocity cracks, upto and including the onset of crack branching. The MCT on the other hand is usually tested with constant displacement, crack-line-wedge-loading and is a standard geometry for crack arrest

measurements. The intermediate range of crack speeds can be investigated with the Ring segment.

Specimens were fabricated from 12.7 mm thick sheets of a brittle, birefringent polyester, Homalite 100, which has been used extensively for model studies of brittle fracture. A notch was saw-cut into the specimen and the tip of this starter notch was blunted so that the specimen could be loaded to a high initial value of K before failure. The specimen and loading fixture were then placed on the optical bench of a high-speed, multi-flash camera of the Cranz-Schardin type. After loading to the desired value of K, the crack was initiated by pulling a sharp knife across the tip of the blunted starter notch. The crack, as it started to propagate, cut a line of silver conducting paint and this triggered the spark gap camera. The camera was typically operated at framing rates of 33,000 frames/second for Ring and MCT tests and at 80,000 frames/second for SEN tests. The optical arrangement of the camera and a set of sixteen photographs from a crack propagation experiment are shown in Figures 5 and 6, respectively. The subsequent sections of this paper discuss the results from one test for each of the three specimen geometries. These results are representative of the observations made during several tests conducted with each geometry.

Results for the SEN Specimen: The results for the analysis of the experimental patterns shown in Figure 6 are presented in Figure 7. Data has been shown only for Frames 1-12 since Frames 13-16 were recorded subsequent to the occurrence of crack branching. The stress intensity factor was observed to increase monotonically with crack length until the crack attempted to branch, at which point K stabilized until successful branching occurred. The leading non-singular coefficients, D_o and C_1, are also shown in Figure 7 (in dimensionless form). These terms vary systematically with crack length and also display a change in behavior when the crack attempts to branch. This result is of particular interest because it suggests that a branching criterion should be based on some combination of the values of K and the leading non-singular term(s).

Results for the MCT Specimen: As stated previously, this specimen geometry is being used to study crack arrest. The results shown in Figure 8 clearly show the sharply decreasing nature of the K-field in this geometry and crack arrest occurred almost at the end of the specimen in this particular experiment. The non-singular terms changed systematically with crack length and the trends show good agreement with results obtained from static analyses of this geometry [17]. As would be expected, terms such as C_1 increase sharply as the crack approaches the specimen boundary and moves into a stronger bending field.

Results for the Ring Specimen: In the example discussed here, the crack was initiated at a high K value and propagated across the specimen without arresting. Crack propagation started at a velocity of $c/c_2 \sim 1/3$ and decreased slowly to about $c/c_2 \sim 1/15$ before the crack came to the end of the specimen. From Figure 9, K dropped from about twice K_{Im} to a value approximately equal to K_{Im}. The range of crack velocities obtained thus covered the entire range of crack speeds from high, constant velocity propagation to very close to arrest. Crack initiation at a lower initial K value was used in other experiments to produce arrest in other tests with this geometry. In terms of its crack speed and K behavior, this specimen starts in the range typical of the SEN geometry and undergoes a transition to the MCT case as the crack length increases. A similar trend is seen in the non-singular coefficients also, with D_o moving from small negative to large positive values and C_1 going from small positive to large negative values.

Relationship Between Crack Speed and K ($\dot{a}$-K): Figure 10 summarizes the results for K versus crack speed in a dimensionless form for the test results

reported here. The gamma-shaped curve is typical of those reported by other investigators and the analysis techniques used here result in substantially decreased scatter and thus lead to a greater degree of confidence in the results. These results indicate that K as a function of crack speed may in fact be a material property and this, combined with the greater accuracy obtained, is of importance in situations where such results are used as inputs to large finite-element computer codes used to predict crack extension behavior in complex structures [3].

SUMMARY AND DISCUSSION

An analytical model and a numerical technique have been presented which together allow an accurate representation of the stress state in a large region around the tip of a propagating crack. The crack propagation behavior in three different specimen geometries has been discussed and results have been presented for the entire range of crack behaviors from crack branching to crack arrest. In addition to illustrating trends in K typical of each geometry, the leading non-singular terms in the series stress field representation have been shown to exhibit systematic but different behaviors in each specimen. The results and methodology presented here provide a means of systematically studying the relationships between crack branching and the values of K, σ_{ox}, and possibly, further non-singular terms.

ACKNOWLEDGEMENTS

The authors are grateful to Drs. G.R. Irwin, R.J. Sanford, and W.L. Fourney for the advice and encouragement that has made this work possible. This research has been supported by NRC and ORNL at the University of Maryland and by NSF at the University of Rhode Island.

REFERENCES

1. Sanford, R.J., Mech. Res. Comm., 6, 289-294 (1979).
2. Irwin, G.R., et al., NUREG/CR-1455, U.S. NRC Report (1980).
3. Fourney, W.L., Chona, R. and Sanford, R.J., Proceedings of the Workshop on Dynamic Fracture, California Inst. of Tech., Pasadena, CA (Feb 1983).
4. Etheridge, J.M. and Dally, J.W., J. Str. Anal., 13 (2), 91-94 (1978).
5. Rossmanith, H.P. and Irwin, G.R., Analysis of Dynamic Crack-Tip Stress Patterns, University of Maryland Report (July 1979).
6. Chona, R., Irwin, G.R. and Shukla, A., J. Str. Anal., 17 (2), 79-86 (1982).
7. Rossmanith, H.P. and Chona, R., Advances in Fracture Research ICF5, 2507-2516 (1981).
8. Sanford, R.J. and Dally, J.W., Engr. Frac. Mech., 11, 621-633 (1979).
9. Barker, D.B., Sanford, R.J. and Chona, R., Proceedings of the 1983 SESA Spring Meeting, Cleveland, Ohio, 445-448 (May 1983).
10. Dally, J.W., Experimental Mechanics, 19 (10), 349-361 (1979).
11. Kobayashi, A.S., et al., ASTM STP 627, 95-108 (1977).
12. Irwin, G.R., Lehigh University Lecture Notes (1968).
13. Irwin, G.R., Proceedings SESA, XVI, 93-96 (1958).
14. Liebowitz, H., et al., Engr. Frac. Mech., 10, 315-335 (1978).
15. Whitman, G.D. and Bryan, R.H., NUREG/CR-2751/Volume 2 (ORNL/TM-8369/v2), U.S. NRC Report, 47-53 (1982).
16. Sanford, R.J. and Chona, R., ASTM Symposium on Chevron-Notched Specimens, Lousville, Kentucky (April 1983) -- ASTM STP in Press.
17. Chona, R., Irwin, G.R. and Sanford R.J., ASTM STP 791, I-3 - I-23 (1983).
18. Chona, R., Fourney, W.L. and Shukla, A., Proceedings of the 1982 SESA/JSME Joint Conference on Experimental Mechanics, Hawaii, 1092-1095 (May 1982).
19. Ramulu, M., Kobayashi, A.S., Kang, B.S.-J. and Barker, D.B., Proceedings of the 1983 SESA Spring Meeting, Cleveland, Ohio, 183-186 (May 1983).

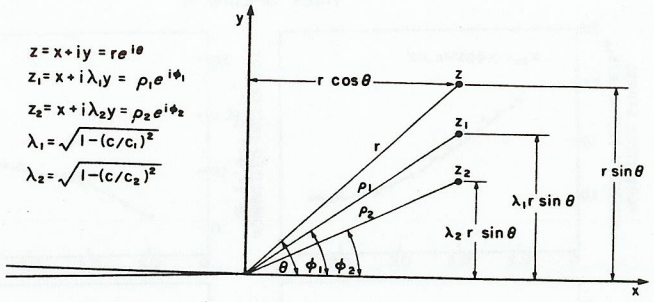

Figure 1 Coordinate systems and transformation relations used in the constant crack speed analysis

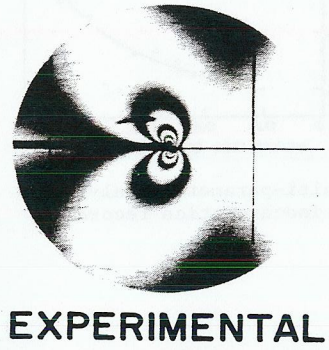

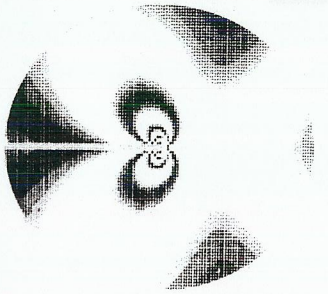

Figure 2

Experimental and reconstructed (computer-generated) fringe patterns for a/W = 0.52 in a Ring segment

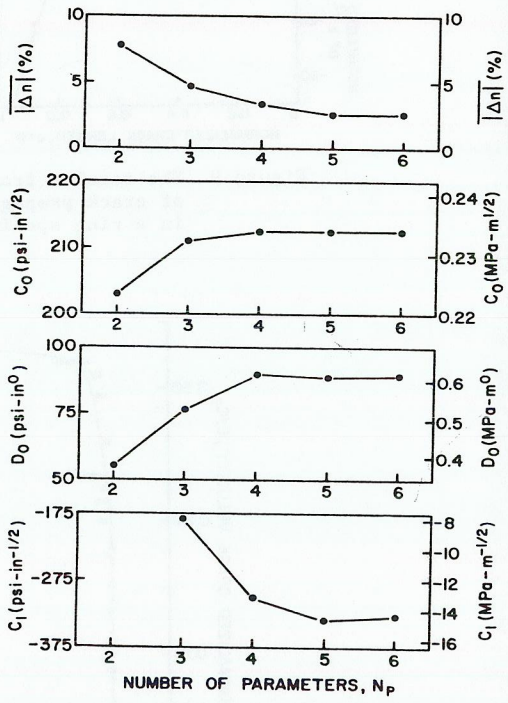

Figure 3

The changes (with increasing order of analysis model) in the error term and leading series coefficients for the fringe pattern shown in Figure 2

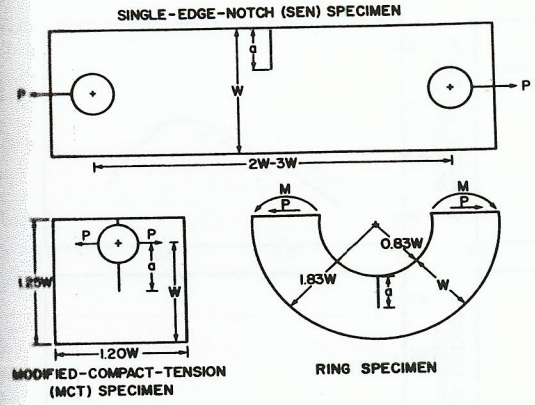

Figure 4

The specimen geometries and relative specimen sizes used in this study

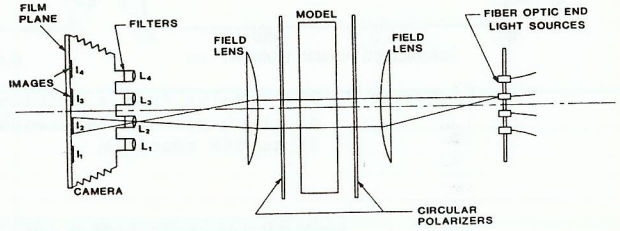

Figure 5

The optical arrangement of a Cranz-Schardin type multiple spark gap camera

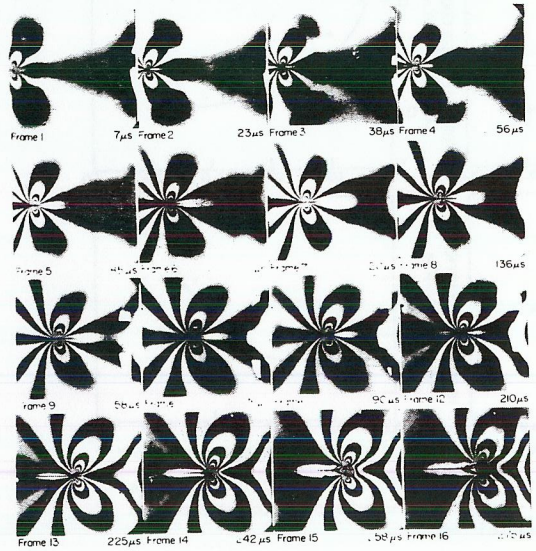

Figure 6

A set of sixteen high speed photographs recorded during a typical crack propagation experiment performed with a Single-Edge-Notch specimen

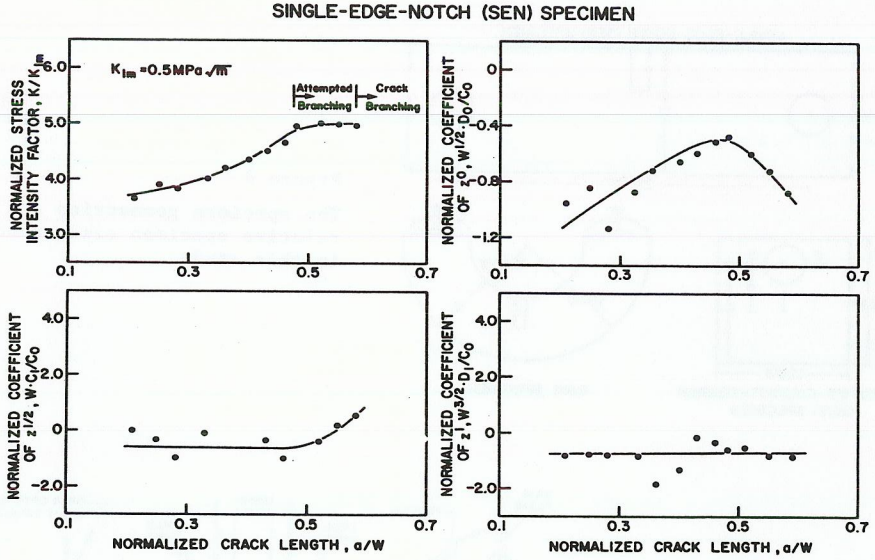

Figure 7 The results from a multi-parameter analysis of crack propagation isochromatics recorded in an SEN specimen

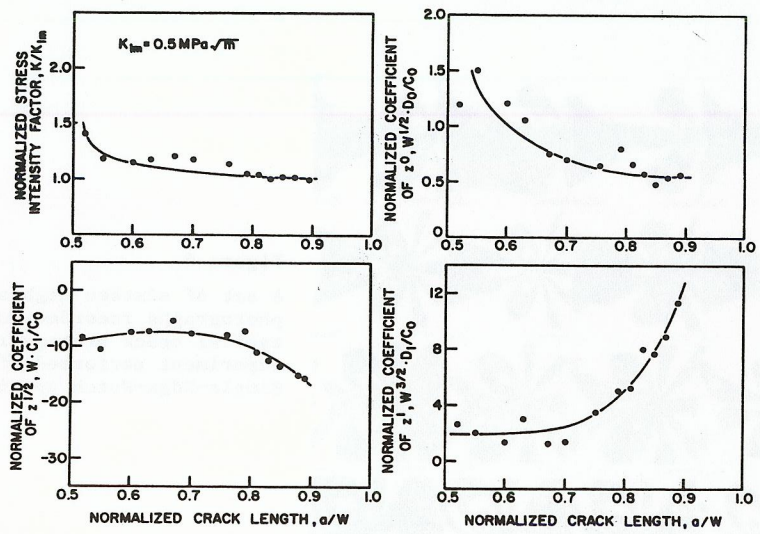

Figure 8 The results from a multi-parameter analysis of crack propagation isochromatics recorded in an MCT specimen

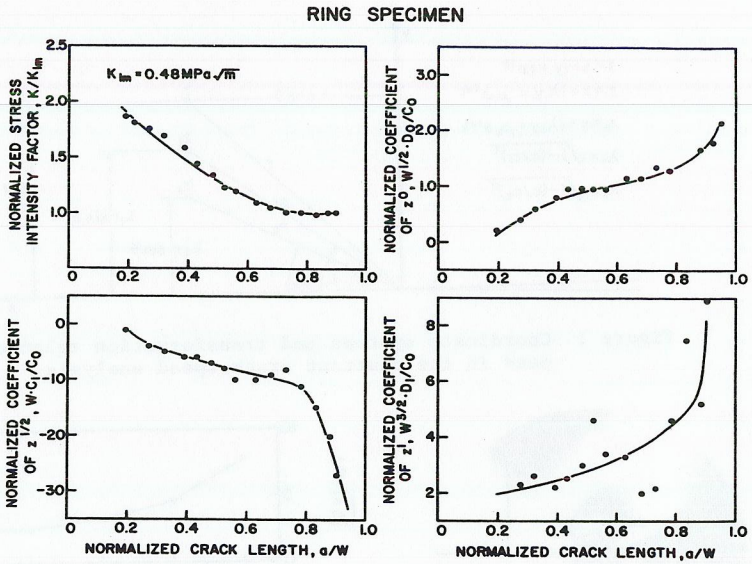

Figure 9 The results from a multi-parameter analysis of crack propagation isochromatics recorded in a ring specimen

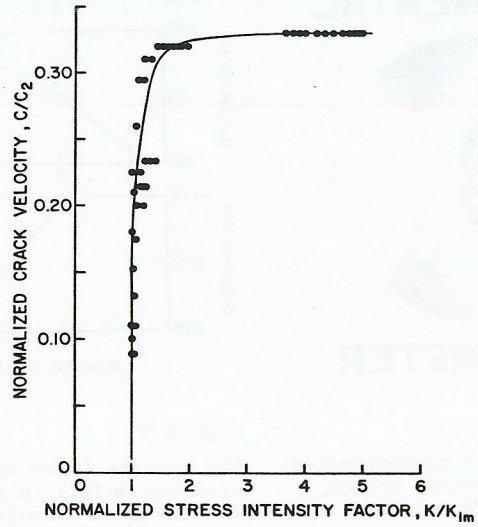

Figure 10 The results for crack speed as a function of stress intensity factor from the three tests shown in Figures 7, 8, and 9